HHS Public Access

Author manuscript

Nat Mater. Author manuscript; available in PMC 2009 June 01.

Published in final edited form as:

Nat Mater. 2008 December ; 7(12): 1003–1010. doi:10.1038/nmat2316.

Accordion-Like Honeycombs for Tissue Engineering of Cardiac Anisotropy

George C. Engelmayr Jr.[1], **Mingyu Cheng**[1], **Christopher J. Bettinger**[2,4], **Jeffrey T. Borenstein**[4], **Robert Langer**[1,3], and **Lisa E. Freed**[1,#]

[1]Harvard-MIT Division of Health Sciences and Technology, Massachusetts Institute of Technology, 77 Massachusetts Avenue, E25-330, Cambridge, MA 02139, USA

[2]Department of Materials Science and Engineering, Massachusetts Institute of Technology, 77 Massachusetts Avenue, E25-330, Cambridge, MA 02139, USA

[3]Department of Chemical Engineering, Massachusetts Institute of Technology, 77 Massachusetts Avenue, E25-330, Cambridge, MA 02139, USA

[4]Biomedical Engineering Center, Charles Stark Draper Laboratory, 555 Technology Square, Cambridge, MA 02139, USA

Abstract

Tissue engineered grafts may be useful in myocardial repair, however previous scaffolds have been structurally incompatible with recapitulating cardiac anisotropy. Utilizing microfabrication techniques, a novel accordion-like honeycomb microstructure was rendered in poly(glycerol sebacate) to yield porous, elastomeric 3-D scaffolds with controllable stiffness and anisotropy. Accordion-like honeycomb scaffolds with cultured neonatal rat heart cells demonstrated utility via: (1) closely matched mechanical properties compared to native adult rat right ventricular myocardium, with stiffnesses controlled by polymer curing time; (2) heart cell contractility inducible by electric field stimulation with directionally-dependent electrical excitation thresholds ($p<0.05$); and (3) greater heart cell alignment ($p<0.0001$) than isotropic control scaffolds. Prototype bilaminar scaffolds with 3-D interconnected pore networks yielded electrically excitable grafts with multi-layered neonatal rat heart cells. Accordion-like honeycombs can thus overcome principal structural-mechanical limitations of previous scaffolds, promoting the formation of grafts with aligned heart cells and mechanical properties more closely resembling native myocardium.

Keywords

myocardial repair; heart; cardiomyocyte; regenerative medicine; biomaterial; biomimetic; microfabrication; excimer laser; microablation; elastomer

[#]*Correspondence to:* Lisa E. Freed, MD, PhD, Massachusetts Institute of Technology, 77 Massachusetts Avenue, Building E25, Room 330, Cambridge, MA 02139, USA, Tel: 617-452-2603, Fax: 617-258-8827, Email: Lfreed@mit.edu.

COMPETING FINANCIAL INTERESTS

The authors declare they have no competing financial interests

Ventricular myocardium is a richly vascularized, quasi-lamellar tissue in which functional syncytia of cardiomyocytes (i.e., cardiac muscle fibers) are interwoven within collagen. Hierarchically, cardiac muscle fibers are surrounded and coupled by endomysial collagen sheaths1 that are bundled within a honeycomb-like network of undulated perimysial collagen fibers2. These features yield directionally-dependent electrical and mechanical properties3 collectively termed cardiac anisotropy (Fig 1). However, in developing tissue engineered grafts for myocardial repair, it has become apparent that previous three-dimensional (3-D) scaffold materials are structurally and mechanically incompatible with the formation of a fully biomimetic tissue. Isotropic collagen foams and gels yield isolated regions of cardiomyocyte alignment, requiring external stimuli such as non-homogeneous boundary constraints4, cyclic stretch5, 6, or electrical stimulation7 to guide parallel orientation; stiff scaffolds such as nonwoven poly(glycolic acid) 8, 9 tend to resist all but small amplitude, largely isometric contractility; and hydrogels, while capable of soft tissue-like compliance10, can be difficult to suture11 and are often too weak to support physiologic loads12. Conceptually appealing would be a scaffold microstructure borrowing more closely from nature's lessons. Indeed, Ott et al.13 recently demonstrated that decellularized adult rat hearts retaining anisotropic structural and mechanical properties could provide a scaffold for cultured neonatal rat heart cells to regenerate nascent pump function. In the current study we sought to microfabricate biomimetic scaffolds with anisotropic structural and mechanical properties from a synthetic bioresorbable elastomer. In particular, we reasoned accordion-like honeycomb scaffolds exhibiting distinct preferred (PD) and orthogonal, cross-preferred (XD) material directions could potentially: (1) match the anisotropic in-plane mechanical response of native myocardium within the physiologic regime, (2) provide low in-plane resistance to contraction, and (3) provide an inherent structural capacity to guide cardiomyocyte orientation in the absence of external stimuli.

The accordion-like honeycomb was designed by overlapping two 200 × 200 μm square pores oriented at 45 degrees (i.e., diamonds) in a pattern to leave a planar network of undulated, 50 μm wide struts (Figs. 2a,b). To assess the utility of accordion-like honeycomb scaffolds in myocardial tissue engineering, poly(glycerol sebacate) (PGS) was chosen as the material of construction for its rubber-like elasticity14 and structure-preserving, gradual degradation (i.e., via surface hydrolysis, with a slow, linear decrease in mechanical strength of ~8% per week *in vivo*)15. Initial PGS curing conditions of 16 h at 160°C were chosen based on previous PGS soft lithography studies16, 17. Mechanical testing of the bulk 16h/160°C PGS yielded effective stiffness (E_{PGS}), ultimate tensile strength (UTS_{PGS}), and strain-to-failure (εf_{PGS}) values of 2116 ± 100 kPa, 793 ± 117 kPa, and 0.69 ± 0.15, respectively. Accordion-like honeycomb scaffolds were fabricated from PGS membranes by excimer laser microablation. A membrane thickness of ~250 μm was chosen to mitigate mass transport limitations, based on our previous modeling analyses of oxygen diffusion through solid PGS17 and tissue engineered myocardium18. Excimer laser microablation yielded well-defined features comparable to the design (Fig. 2a–c). Accordion-like honeycomb scaffolds were found to be anisotropic when tested under uniaxial tension, with different effective stiffnesses in the PD and XD directions (E_{PD} = 195 ± 8 kPa versus E_{XD} = 57 ± 3 kPa, $p < 0.0001$, with an associated anisotropy ratio E_{PD}/E_{XD} of 3.4 ± 0.2).

To determine if these stiffness values were appropriate, specimens of adult rat right (RV) and left (LV) ventricular myocardium were tested in the circumferential (CIRC) and longitudinal (LONG) directions, and effective stiffnesses (E_{CIRC}, E_{LONG}) were obtained in the linear, physiologic strain regime of ± 0.1519–21 (Fig. 1c). Of note, while organ-level cardiac muscle structures22 and transmural variations in muscle fiber orientation23 are complex, we defined CIRC and LONG axes that respectively corresponded to the epicardial surface of the heart sectioned transversely and longitudinally (i.e., apex-to-base) as in previous tissue engineering13, mechanical19, 21 and anatomical2 studies. Compared to 16h/160°C PGS accordion-like honeycomb scaffolds, adult rat RV myocardium (E_{CIRC} = 54 ± 8 kPa versus E_{LONG} = 20 ± 4, $p < 0.01$, and E_{CIRC}/E_{LONG} = 2.8 ± 0.5) was similarly anisotropic, but less stiff. Adult rat RV myocardium was more anisotropic and compliant than its LV counterpart (E_{CIRC} = 157 ± 14 kPa versus E_{LONG} = 84 ± 8, $p < 0.01$, and E_{CIRC}/E_{LONG} = 2.1 ± 0.4), leading us to focus on approximating RV myocardium mechanical properties. We reasoned that RV myocardial grafts with the potential to grow, regenerate, and remodel could ultimately lead to new treatments for congenital heart defects, which typically affect the right ventricle24, 25, as well as for RV infarctions that frequently complicate LV infarctions26 and are associated with substantial first-year mortality27.

We next sought a better match between the magnitudes of E_{PD} and E_{XD} of accordion-like honeycomb scaffolds and E_{CIRC} and E_{LONG} of adult RV myocardium by reducing the PGS curing time28. Note that non-porous PGS was recently tailored for myocardial applications by varying curing temperature29. PGS was cured at 160°C for times ranging from 4 to 16 h, yielding a standard curve with a linear dependence of E_{PGS} on curing time within the tested range (Fig. 2d). Utilizing this standard curve with the ratios E_{PD}/E_{PGS} = 0.092 ± 0.006 and E_{XD}/E_{PGS} = 0.027 ± 0.002 calculated from the 16h/160°C data, we predicted 7.5 h curing would yield E_{PD} and E_{XD} values of ~77 and ~22 kPa, respectively, closely matching the corresponding values of E_{CIRC} and E_{LONG} of adult RV myocardium. As predicted, mechanical testing of the 7.5h/160°C PGS yielded E_{PGS} = 825 ± 62 kPa, and accordion-like honeycomb scaffolds fabricated and wetted for 24 h yielded E_{PD} = 83 ± 2 kPa kPa versus E_{XD} = 31 ± 1 kPa ($p < 0.0002$), and E_{PD}/E_{XD} = 2.7 ± 0.1 kPa (Table 1; Supplementary Information, Fig. S1). Strain-to-failure, εf, was ~1.6 for accordion-like honeycomb scaffolds made of 7.5h/160C PGS (Table 1). By comparison, an isotropic PGS foam we used previously30, 31 appeared less suitable for adult rat RV myocardium, with E_{FOAM} ~ 2-to-9 kPa and εf_{FOAM} ~ 0.4-to-0.8 (ranges estimated from Fig. 9 of Crapo et al. 32).

To assess longer term mechanical stability, accordion-like honeycomb scaffolds made of 7.5h/160°C PGS were placed in a fatigue bath (Supplementary Information, Fig. S2) and subjected to *in vitro* cyclic stretch mimicking physiologic loading5, 6, 33. Specimens were subjected to cyclic loading at 1 Hz and peak strain of 0.1 (i.e., 10%) for 1 week in buffered saline at room temperature. Fatigued scaffolds yielded: E_{PD} = 46 ± 4 kPa versus E_{XD} = 19 ± 0.8 kPa ($p<0.02$), with E_{PD}/E_{XD} = 2.4 ± 0.2 (Table 1; Supplementary Information, Fig. S3). Compared to adult rat RV myocardium, fatigued scaffolds exhibited similar mechanical properties (Table 1) except for higher εf values. Compared to scaffolds maintained statically in water for 24 h to 3 weeks, fatigued scaffolds exhibited similar mechanical properties except for a lower E_{PD} (Table 1; Supplementary Information, Fig. S1).

To assess the mechanical properties with cultured neonatal rat heart cells, scaffolds made of 7.5h/160°C PGS (10 × 5 mm, n=5 per group) were autoclave-sterilized, seeded with cells isolated from neonatal rat ventricles, and cultured *in vitro* for 1 week. Grafts yielded an attenuated anisotropic mechanical response (Fig. 2e), with E_{PD} = 32 ± 2 kPa versus E_{XD} = 19 ± 4 kPa ($p>0.05$) and E_{PD}/E_{XD} = 1.9 ± 0.3 (Table 1; Supplementary Information, Fig. S4). Compared to adult rat RV myocardium, accordion-like honeycomb scaffolds with cultured heart cells exhibited a lower E_{PD} and higher εf values. Compared to wetting for 24 h to 3 weeks, scaffolds with heart cells exhibited a lower E_{PD} and insignificantly higher εf values (Table 1). Of note, autoclaving did not significantly change PGS mechanical response (Supplementary Information, Fig. S5). Together, these data suggested that *in vitro* culture of heart cells reduced E_{PD}, possibly due to a combination of scaffold biodegradation and extracellular matrix deposition. These effects will need to be considered in future studies if scaffold mechanical properties are to be matched to adult rat RV myocardium post-culture.

To compare grafts based on accordion-like honeycomb scaffolds of varying effective stiffness, neonatal rat heart cells were seeded on scaffolds made of PGS cured for 7.5, 12, and 16 h (5× 5 mm, n=6 per group). After 1 week *in vitro* culture, the majority of pores were filled with neonatal rat heart cells grossly aligned along the PD direction, as shown by confocal microscopy of grafts labeled for filamentous (F-) actin (Fig. 3a,b; Supplementary Information, Fig. S6). Note that F-actin labeling principally identified stress fibers in the cardiac fibroblast fraction of the cultured neonatal heart cells. Higher magnification images demonstrated some elongated cells (Fig. 3c) and cross-striations (Fig. 3d) similar but significantly less developed than those characteristic of adult rat RV myocardium (Fig. 3e). To assess graft cellularity, DNA contents were measured, found not to depend significantly on PGS curing time, and yielded an average of 0.766 ± 0.043 mg DNA per gram wet weight comparable to our previous 1 week study of engineered myocardial grafts9.

Electrophysiological assessment30, 31, 34, 35 demonstrated synchronous contractions in all scaffold groups, with all grafts capable of being paced by electrical field stimulation at up to at least 2 Hz (Supplementary Information, Video S1). Excitation thresholds (ET) were found not to depend significantly on PGS curing time. Hence, these data were pooled to yield a directional dependence of ET for a given scaffold orientation with respect to the electric field. In particular, ET was 11 ± 4% lower when measured with the scaffold PD oriented parallel versus perpendicular to the applied electric field (ET_{PD}= 1.05 ± 0.02 V versus ET_{XD}= 1.19 ± 0.04 V, $p < 0.01$). This was consistent with reports in which ET for cultured adult guinea pig36 and canine37 cardiomyocytes depended on the orientation of the elongated cells with respect to the electric field, with ~50% lower ET with the long cell axis parallel versus perpendicular.

Separate experiments were undertaken to compare accordion-like (Fig. 4a), square (200 × 200 μm; Fig. 4b), and rectangular (400 × 200 μm; Fig. 4c) honeycomb scaffolds fabricated from 16 h/160°C PGS. These scaffolds exhibited different degrees of mechanical anisotropy (Fig. 4d). Accordion-like honeycombs (E_{PD} = 195 ± 8 kPa, E_{XD} = 57 ± 3 kPa, and E_{PD}/E_{XD} = 3.4 ± 0.2) and rectangular honeycombs (E_{PD} = 206 ± 21 kPa versus E_{XD} = 117 ± 16 kPa, $p < 0.01$, and E_{PD}/E_{XD} = 1.8 ± 0.3) were anisotropic while square honeycombs were

isotropic ($E_{PD} = E_{XD} = 270 \pm 22$ kPa; $E_{PD}/E_{XD} = 1$). These results confirmed that of the scaffolds tested, the accordion-like honeycomb scaffold exhibited anisotropic mechanical properties most closely resembling adult rat RV myocardium (Table 1).

To assess whether electrical ET was influenced by scaffold microstructure, honeycomb scaffolds with accordion-like, square, and rectangular pores (5×5 mm, n=4 per group) were autoclave-sterilized, seeded with neonatal rat heart cells, and cultured *in vitro* for 1 week. Based on our finding that co-cultured cardiac fibroblasts enhanced assembly of contractile grafts30, scaffolds were sequentially seeded with cardiac fibroblasts followed by neonatal rat heart cells enriched for cardiomyocytes. As few as 4 days after seeding, spontaneous contractions were observed in all groups. After 1 week culture, the majority of pores were filled by neonatal rat heart cells and the grafts could be synchronously paced at up to 4 Hz. ET depended significantly on the orientation of the scaffold PD with respect to the electric field (Fig. 4e). Anisotropic accordion-like and rectangular honeycomb scaffolds respectively had 12 ± 1% and 17 ± 2% lower ET values when the scaffold PD was aligned parallel to the electric field ($p = 0.02$), whereas no consistent dependence was observed in isotropic square honeycombs (data not shown), similar to isotropic electrophysiologic properties observed by our group on randomly oriented nonwoven poly(glycolic acid) scaffolds38.

To assess whether heart cell alignment was influenced by scaffold microstructure, F-actin filament orientation39 was quantified by Fast Fourier Transform (FFT)-based image analysis of confocal micrographs taken at a depth of ~30 μm from the grafts (Fig. 3b; Supplementary Information, Fig. S7–S9). Adult RV myocardium imaged from the epicardial surface was analyzed for comparison (Supplementary Information, Fig. S10). An orientation index (OI) was defined as the angular increment centered about the mean encompassing 50% of the total (F-actin filament) population (i.e., lower OI indicates a tighter distribution about the mean and more parallel alignment)39–41. Values of OI for adult rat RV myocardium were respectively 27 ± 9% and 31 ± 10% lower than for accordion-like and rectangular honeycombs ($p<0.05$) (Figs. 4f,g). Values of OI measured for accordion-like and rectangular honeycombs were respectively 37 ± 6% and 33 ± 6% lower than for isotropic square honeycombs ($p<0.0001$) (Figs. 4f,g), indicating that each of the two anisotropic scaffolds possessed an inherent structural capacity to guide preferential heart cell alignment along the PD material direction. Moreover, high and similar OI values (85 ± 5° versus 81 ± 2°, $p>0.05$) were measured for square honeycomb scaffolds consisting of 1:1 aspect ratio pores as well as for a previously used porogen-leached PGS foam28, 30 that we fabricated and analyzed for comparison (Supplementary Information, Fig. S11). Of note, similar OI values (58 ± 4° versus 54 ± 1°, $p>0.05$) were obtained for accordion-like honeycombs independent of scaffold stiffness (7.5 h/160°C versus 16 h/160°C) and cell seeding method (unseparated neonatal rat heart cells versus serially seeding with cardiac fibroblasts plus cardiomyocyte-enriched heart cells) suggesting that, under the conditions tested, pore geometry and not E_{PGS} or seeding method likely dominated cell orientation.

While ~250 μm thick honeycomb scaffolds provide a model for systematic *in vitro* studies, they are too thin to address reconstruction of full-thickness myocardium, except perhaps via a polysurgery strategy42. Moreover, with its transmural distribution of cardiac muscle fiber orientations19, 22, 23, the quasi-lamellar structure of ventricular myocardium seems to

demand an equivalently adaptive out-of-plane scaffold structure. As a first step toward addressing these limitations, prototype bilaminar honeycomb scaffolds of greater thickness (~400 μm) with interconnected 3-D square pore networks were fabricated by partially microablating a lateral array of troughs in one PGS lamina, overlaying a second lamina, microablating an array of top-to-bottom pores through both lamina, and then stabilizing the resultant bilaminar honeycomb scaffold by thermal cross-linking17, 43 (Fig. 5a,b). In a preliminary study, unseparated neonatal rat heart cells were cultured for 1 week on bilaminar scaffolds. Cellular penetration of and interconnectivity between the top-to-bottom and lateral pores were observed in histological cross-section (Figs. 5c) as well as in serial, through-thickness confocal sections (Fig. 5d). These preliminary studies suggest our bilaminar scaffolds with 3-D interconnected pore networks can enable the formation of multi-layered tissue structures from neonatal rat heart cells, thereby extending recent demonstrations that 2-D microfabricated materials can guide the behavior of cultured heart cells44, 45. These findings further suggest that combined excimer laser microablation and lamination might be useful in fabricating honeycomb scaffolds of greater thickness from discrete, potentially offset lamina, with the caveat that thicker scaffolds would likely require perfusion to maintain cardiomyocyte viability35, 46–48. Future studies will also focus on programming the excimer laser to generate the more complex arrays of troughs required for the assembly of a bilaminar accordion-like honeycomb scaffold.

To the best of our knowledge, this is the first report of a scaffold incorporating an accordion-like honeycomb microstructure. In particular, the accordion-like honeycomb scaffold demonstrated the novel ability to yield tissue engineered grafts with closely matched anisotropic mechanical properties compared to adult rat RV myocardium, while simultaneously promoting the preferential orientation of cultured neonatal rat heart cells in the absence of external stimuli. Matching of tissue mechanical properties was enabled by the materials engineering approach we introduced, in which a standard curve (Fig. 2d) of PGS stiffness versus curing time was established at constant temperature and utilized in conjunction with measured ratios of scaffold-to-membrane stiffness to predict *a priori* the required PGS curing time. Also introduced was the use of excimer laser microablation in PGS microfabrication, which allowed creation of open, closely spaced (~50 μm apart) pores with variable, precisely controlled geometries in ~250 μm thick PGS membranes, with the limitation that pores exhibited a slight top-to-bottom taper typical of laser drilling49 (Fig. 2c, 5a,b). Feature resolution with excimer laser microablation was higher than our previous study wherein a carbon dioxide laser created more widely spaced (>410 μm apart), larger (>370 μm diameter) culture medium flow channels of cylindrical geometry in 2 mm thick PGS foam31. PGS membrane thickness with excimer laser microablation was 5-fold higher than our previous study wherein replica molding created more widely spaced (i.e., 175 μm apart), small (50 μm) pores in thin (45 μm) PGS membranes50. Although electrical field stimulation did induce synchronous contractions of neonatal rat heart cells cultured on accordion-like honeycomb scaffolds, these contractions remained largely isometric under the conditions tested. Reduction in scaffold in-plane compressive resistance towards that of collagen foams7, 34, 35, 46 and PGS foams30, 31, (e.g. by further reducing E_{PGS} or strut width of accordion-like honeycomb scaffolds) is expected to result in macroscopic contractility (i.e., fractional area change) of engineered myocardial grafts. Also, use of soft

lithography for surface micropatterning of the PGS16, 17, 43 prior to excimer laser microablation, and *in vitro* application of mechanical5, 6 or electrical7 stimulation are expected to further increase orientation of cultured neonatal rat heart cells.

In conclusion, we have shown that accordion-like honeycomb scaffolds can overcome principal structural-mechanical limitations of scaffolds for myocardial tissue engineering by promoting the formation of grafts with preferentially aligned neonatal rat heart cells and mechanical properties more closely resembling adult rat RV myocardium. Generalized to an enabling technology for structural biomimicry, libraries of bioresorbable honeycombs exhibiting graded microstructural features could likewise be generated, paving the way toward further integration of tissue-specialized scaffolds into advanced tissue engineering strategies.

METHODS (see also Supplementary Information)

Excimer laser microablation

PGS membranes (~250 μm thick) on silicon wafers16 were situated on the x-y stage (accuracy ± 1 μm) of a Rapid X® 1000 system (Resonetics, Nashua, NH) with a 248 nm Krypton Fluoride LPX200 excimer laser (Coherent-Lambda Physik, Santa Clara, CA). Pores were patterned via G-code programs. For highly cross-linked PGS (16 h/160°C), a power of 350 mJ, burst frequency of 500/sec and burst count of 1000 were used. For partially cross-linked PGS (e.g., 7.5h/160°C), the respective burst frequency and burst count were 25/sec, and 100. Scaffolds were loosened from wafers in deionized water (24 h) and 70% ethanol (24 h). Bilaminar scaffolds (~400 μm) with 3-D pore networks were fabricated by microablating a lateral array of troughs in one PGS lamina (burst spacing of 0.01 sec; table speed of 0.5 mm/sec), overlaying a second PGS lamina, microablating top-to-bottom pores through both lamina (burst frequency of 500/sec; burst count of 2000), and then stabilizing the resultant scaffold by thermally cross-linking17 via autoclaving (121°C for 30 min).

Heart cell culture on microfabricated PGS scaffolds

Cells were obtained from 2-day old neonatal rat hearts via an Institute-approved protocol as described8 (see Supplementary Information, Methods). In studies of PGS scaffolds with varying effective stiffness and prototype bilaminar scaffolds (5 mm × 5 mm for imaging; 10 mm × 5 mm for mechanics), scaffolds were autoclave-sterilized and seeded with freshly harvested, unseparated neonatal rat heart cells at ~36×10^6 cells/cm^2. In brief, 10 mL of cell suspension were added to a vent-capped 50 mL tube (Product # 91253; TPP, Trasadingen, Switzerland) containing one scaffold, and tubes were placed in a 37°C/5% CO_2 humidified incubator and gently mixed (8 rpm) using a rotisserie (Labquake, Barnstead-Thermolyne, Dubuque, IA). After 4 days, culture media were replaced and culture was continued statically for 3 more days. In studies of 16h/160°C PGS scaffolds with varying pore structures, scaffolds (5 mm × 5 mm) were autoclave-sterilized and sequentially seeded30 first with cardiac fibroblasts at ~1×10^6 cells/cm^2, followed by a heart cell population enriched for cardiomyocytes at ~36×10^6 cells/cm^2. In brief, 10 mL of cardiac fibroblast cell suspension was added to a 50 mL tissue culture tube containing a single scaffold and cultured with gentle mixing as described above. After 5 days, cardiomyocyte-enriched heart

cells were added, and after an additional 3 days, grafts were transferred to petri dishes (Costar Ultra Low Attachment; Corning, Corning, NY) (one per 35 mm well) and cultured statically for 4 more days. Culture media (6 mL/well) were replaced every 2 days.

Electrophysiologic assessement

Specimens were assessed using our previous method, wherein an electrical pulse generator applied biphasic square waveforms at 1, 2, 3, and 4 Hz to a specimen positioned between two carbon rod electrodes within an environmentally-controlled, perfused test chamber[34, 35]. Excitation threshold (ET) was defined as the minimum voltage observed to initiate synchronous contractions. Video recordings made at twice the ET used a 30 frame/s video camera (Sony XCD-X710) and Nikon Diaphot microscope at 10X magnification.

Confocal microscopy and cell orientation analysis

Cell orientation was evaluated using confocal laser microscopy with staining of filamentous actin (F-actin)[39] and fast Fourier transform (FFT)-based image analysis[40, 51]. In brief, specimens were rinsed, fixed in 10% neutral buffered formalin (Sigma) for 2 h, rinsed, extracted in 0.2% (v/v) Triton X-100 (Sigma) in PBS for 2 h, rinsed, pre-incubated in 1% (w/v) bovine serum albumin (Sigma) in PBS (BSA buffer) for 2 h, incubated in Alexa Fluor® 488-Phalloidin (2:150 (v/v) dilution; Molecular Probes) for 3 h, rinsed, and then incubated in DRAQ5™(25 μM in PBS; Biostatus Limited, Leicestershire, UK) for 30 min, all at room temperature. Specimens were then rinsed, bulk mounted on glass slides in Vectashield® medium (Vector Laboratories, Burlingame, CA), and cover-slipped. Specimens were imaged with 25X and 100X oil immersion objectives on a Zeiss LSM 510 laser scanning confocal microscope, with F-actin and nuclei pseudo-colored green and blue, respectively. Micrographs of F-actin filaments (i.e., green channel) were analyzed for cell orientation using a Matlab program. FFT image analysis was similar to our previous study[40], and adapted from Ng et al.[51]. See descriptions of FFT in quantifying 2-D fiber network orientation[52] and comparisons of FFT to morphometry[53]. Micrographs taken at ~30 μm from the graft and RV epicardial surfaces were analyzed (n=6 pores; one representative sample per group). Orientation index (OI) was defined as the angular increment centered about the distribution mean encompassing 50% of the population[41]. For random cell orientations OI approaches 90 degrees; for highly aligned cells OI approaches zero.

Statistics

Data were mean ± SEM unless indicated. Calculated parameter errors were determined by propagation of error. Comparisons were made by one-factor (anisotropy ratio) or two-factor (other parameters) ANOVA with Tukey's *post-hoc* test (Statistica v7, StatSoft, Tulsa, OK). A p-value < 0.05 was considered significant.

Supplementary Material

Refer to Web version on PubMed Central for supplementary material.

ACKNOWLEDGMENTS

Funding for this work was provided by NIH NRSA fellowship 1 F32 HL084968-01 (to GCE), a Charles Stark Draper fellowship (to CJB), NASA Grant NNJ04HC72G (to LEF), and NIH Grant DE013023 (to RL). We are indebted to Y. Wang and M. Radisic for advice on porogen-leached PGS scaffolds, S.N. Bhatia, D. Albright, and D. Ward for advice on PGS membrane microfabrication, N. Watson and E. Batchelder for help with confocal and electron microscopy, and S. Kangiser for help with manuscript preparation.

REFERENCES

1. Macchiarelli G, et al. A micro-anatomical model of the distribution of myocardial endomysial collagen. Histol Histopathol. 2002; 17:699–706. [PubMed: 12168777]
2. Hanley PJ, Young AA, LeGrice IJ, Edgar SG, Loiselle DS. 3-Dimensional configuration of perimysial collagen fibres in rat cardiac muscle at resting and extended sarcomere lengths. J Physiol. 1999; 517(Pt 3):831–837. [PubMed: 10358122]
3. Holmes JW, Borg TK, Covell JW. Structure and mechanics of healing myocardial infarcts. Annu Rev Biomed Eng. 2005; 7:223–253. [PubMed: 16004571]
4. Costa KD, Lee EJ, Holmes JW. Creating alignment and anisotropy in engineered heart tissue: role of boundary conditions in a model three-dimensional culture system. Tissue Eng. 2003; 9:567–577. [PubMed: 13678436]
5. Akhyari P, et al. Mechanical stretch regimen enhances the formation of bioengineered autologous cardiac muscle grafts. Circulation. 2002; 106:I137–I142. [PubMed: 12354723]
6. Fink C, et al. Chronic stretch of engineered heart tissue induces hypertrophy and functional improvement. FASEB J. 2000; 14:669–679. [PubMed: 10744624]
7. Radisic M, et al. Functional assembly of engineered myocardium by electrical stimulation of cardiac myocytes cultured on scaffolds. Proc Natl Acad Sci U S A. 2004; 101:18129–18134. [PubMed: 15604141]
8. Bursac N, et al. Cardiac muscle tissue engineering: toward an in vitro model for electrophysiological studies. Am J Physiol Heart Circ Physiol. 1999; 277:H433–H444.
9. Papadaki M, et al. Tissue engineering of functional cardiac muscle: molecular, structural, and electrophysiological studies. Am J Physiol Heart Circ Physiol. 2001; 280:H168–H178. [PubMed: 11123231]
10. Yeo Y, et al. Photocrosslinkable hydrogel for myocyte cell culture and injection. J Biomed Mater Res B Appl Biomater. 2007; 81:312–322. [PubMed: 16969828]
11. Zimmermann WH, et al. Engineered heart tissue grafts improve systolic and diastolic function in infarcted rat hearts. Nat Med. 2006; 12:452–458. [PubMed: 16582915]
12. Feng Z, Matsumoto T, Nakamura T. Measurements of the mechanical properties of contracted collagen gels populated with rat fibroblasts or cardiomyocytes. J Artif Organs. 2003; 6:192–196. [PubMed: 14598103]
13. Ott HC, et al. Perfusion-decellularized matrix: using nature's platform to engineer a bioartificial heart. Nat Med. 2008; 14:213–221. [PubMed: 18193059]
14. Wang Y, Ameer GA, Sheppard BJ, Langer R. A tough biodegradable elastomer. Nat Biotechnol. 2002; 20:602–606. [PubMed: 12042865]
15. Wang Y, Kim YM, Langer R. In vivo degradation characteristics of poly(glycerol sebacate). J Biomed Mater Res A. 2003; 66:192–197. [PubMed: 12833446]
16. Bettinger CJ, Orrick B, Misra A, Langer R, Borenstein JT. Microfabrication of poly (glycerol-sebacate) for contact guidance applications. Biomaterials. 2006; 27:2558–2565. [PubMed: 16386300]
17. Bettinger CJ, et al. Three-dimensional microfluidic tissue-engineering scaffolds using a flexible biodegradable polymer. Advanced Materials. 2006; 18:165-+. [PubMed: 19759845]
18. Radisic M, et al. Oxygen gradients correlate with cell density and cell viability in engineered cardiac tissue. Biotechnol Bioeng. 2006; 93:332–343. [PubMed: 16270298]

19. Chuong CJ, Sacks MS, Templeton G, Schwiep F, Johnson RL Jr. Regional deformation and contractile function in canine right ventricular free wall. Am J Physiol. 1991; 260:H1224–H1235. [PubMed: 2012225]
20. Rappaport D, Adam D, Lysyansky P, Riesner S. Assessment of myocardial regional strain and strain rate by tissue tracking in B-mode echocardiograms. Ultrasound Med Biol. 2006; 32:1181–1192. [PubMed: 16875953]
21. Sacks MS, Chuong CJ. Biaxial mechanical properties of passive right ventricular free wall myocardium. Journal of Biomechanical Engineering. 1993; 115:202–205. [PubMed: 8326727]
22. Kocica MJ, et al. The helical ventricular myocardial band: global, three-dimensional, functional architecture of the ventricular myocardium. Eur J Cardiothorac Surg. 2006; 29(Suppl 1):S21–S40. [PubMed: 16563790]
23. Streeter DD Jr, Spotnitz HM, Patel DP, Ross J Jr, Sonnenblick EH. Fiber orientation in the canine left ventricle during diastole and systole. Circ Res. 1969; 24:339–347. [PubMed: 5766515]
24. Bautista-Hernandez V, et al. Coarctectomy reduces neoaortic arch obstruction in hypoplastic left heart syndrome. J Thorac Cardiovasc Surg. 2007; 133:1540–1546. [PubMed: 17532953]
25. Reinhartz O, et al. Homograft valved right ventricle to pulmonary artery conduit as a modification of the Norwood procedure. Circulation. 2006; 114:1594–1599.
26. Kinch JW, Ryan TJ. Right ventricular infarction. N Engl J Med. 1994; 330:1211–1217. [PubMed: 8139631]
27. Gumina RJ, Murphy JG, Rihal CS, Lennon RJ, Wright RS. Long-term survival after right ventricular infarction. Am J Cardiol. 2006; 98:1571–1573. [PubMed: 17145212]
28. Gao J, Crapo PM, Wang Y. Macroporous elastomeric scaffolds with extensive micropores for soft tissue engineering. Tissue Eng. 2006; 12:917–925. [PubMed: 16674303]
29. Chen QZ, et al. Characterisation of a soft elastomer poly(glycerol sebacate) designed to match the mechanical properties of myocardial tissue. Biomaterials. 2008; 29:47–57. [PubMed: 17915309]
30. Radisic M, et al. Pre-treatment of synthetic elastomeric scaffolds by cardiac fibroblasts improves engineered heart tissue. J Biomed Mater Res A. 2008; 86:713–724. [PubMed: 18041719]
31. Radisic M, et al. Biomimetic approach to cardiac tissue engineering: oxygen carriers and channeled scaffolds. Tissue Eng. 2006; 12:2077–2091. [PubMed: 16968150]
32. Crapo PM, Gao J, Wang Y. Seamless tubular poly(glycerol sebacate) scaffolds: high-yield fabrication and potential applications. J Biomed Mater Res A. 2008; 86:354–363. [PubMed: 17969024]
33. Boublik J, et al. Mechanical properties and remodeling of hybrid cardiac constructs made from heart cells, fibrin, and biodegradable, elastomeric knitted fabric. Tissue Eng. 2005; 11:1122–1132. [PubMed: 16144448]
34. Cheng M, Park H, Engelmayr GC, Moretti M, Freed LE. Effects of regulatory factors on engineered cardiac tissue in vitro. Tissue Eng. 2007; 13:2709–2719. [PubMed: 17708718]
35. Cheng M, Moretti M, Engelmayr GC Jr, Freed LE. Insulin-like growth factor-I and slow, bi-directional perfusion enhance the formation of tissue-engineered cardiac grafts. Tissue engineering. Part A. (In-press; PMID: 18759675).
36. Bardou AL, et al. Directional variability of stimulation threshold measurements in isolated guinea pig cardiomyocytes: relationship with orthogonal sequential defibrillating pulses. Pacing Clin Electrophysiol. 1990; 13:1590–1595. [PubMed: 1704510]
37. Ranjan R, Thakor NV. Electrical stimulation of cardiac myocytes. Ann Biomed Eng. 1995; 23:812–821. [PubMed: 8572431]
38. Bursac N, et al. Cultivation in rotating bioreactors promotes maintenance of cardiac myocyte electrophysiology and molecular properties. Tissue Eng. 2003; 9:1243–1253. [PubMed: 14670112]
39. Engelmayr GC Jr, Papworth GD, Watkins SC, Mayer JE Jr, Sacks MS. Guidance of engineered tissue collagen orientation by large-scale scaffold microstructures. J Biomech. 2006; 39:1819–1831. [PubMed: 16043186]
40. Nichol JW, Engelmayr GC Jr, Cheng M, Freed LE. Co-culture induces alignment in engineered cardiac constructs via MMP-2 expression. Biochem Biophys Res Commun. 2008; 373:360–365. [PubMed: 18559256]

41. Sacks MS, Smith DB, Hiester ED. A small angle light scattering device for planar connective tissue microstructural analysis. Ann Biomed Eng. 1997; 25:678–689. [PubMed: 9236980]
42. Shimizu T, et al. Polysurgery of cell sheet grafts overcomes diffusion limits to produce thick, vascularized myocardial tissues. Faseb J. 2006; 20:708–710. [PubMed: 16439619]
43. Borenstein JT, et al. Microfabrication of three-dimensional engineered scaffolds. Tissue Eng. 2007; 13:1837–1844. [PubMed: 17590149]
44. Camelliti P, Gallagher JO, Kohl P, McCulloch AD. Micropatterned cell cultures on elastic membranes as an in vitro model of myocardium. Nature protocols. 2006; 1:1379–1391. [PubMed: 17406425]
45. Feinberg AW, et al. Muscular thin films for building actuators and powering devices. Science. 2007; 317:1366–1370. [PubMed: 17823347]
46. Radisic M, et al. Medium perfusion enables engineering of compact and contractile cardiac tissue. Am J Physiol Heart Circ Physiol. 2004; 286:H507–H516. [PubMed: 14551059]
47. Dvir T, Benishti N, Shachar M, Cohen S. A novel perfusion bioreactor providig a homogenous milieu for tissue regeneration. Tissue Eng. 2006; 12:2843–2852. [PubMed: 17518653]
48. Dvir T, Levy O, Shachar M, Granot Y, Cohen S. Activation of the ERK1/2 cascade via pulsatile interstitial fluid flow promotes cardiac tissue assembly. Tissue Eng. 2007; 13:2185–2193. [PubMed: 17518740]
49. Dahotre, NB.; Harimkar, SP. Laser fabrication and machining of materials. New York, N.Y.: Springer Science+Business Media; 2008.
50. Neeley WL, et al. A microfabricated scaffold for retinal progenitor cell grafting. Biomaterials. 2008; 29:418–426. [PubMed: 17961646]
51. Ng CP, Hinz B, Swartz MA. Interstitial fluid flow induces myofibroblast differentiation and collagen alignment in vitro. J Cell Sci. 2005; 118:4731–4739. [PubMed: 16188933]
52. Ayres CE, et al. Measuring fiber alignment in electrospun scaffolds: a user's guide to the 2D fast Fourier transform approach. J Biomater Sci Polym Ed. 2008; 19:603–621. [PubMed: 18419940]
53. Sander EA, Barocas VH. Comparison of 2D fiber network orientation measurement methods. J Biomed Mater Res A. 2008

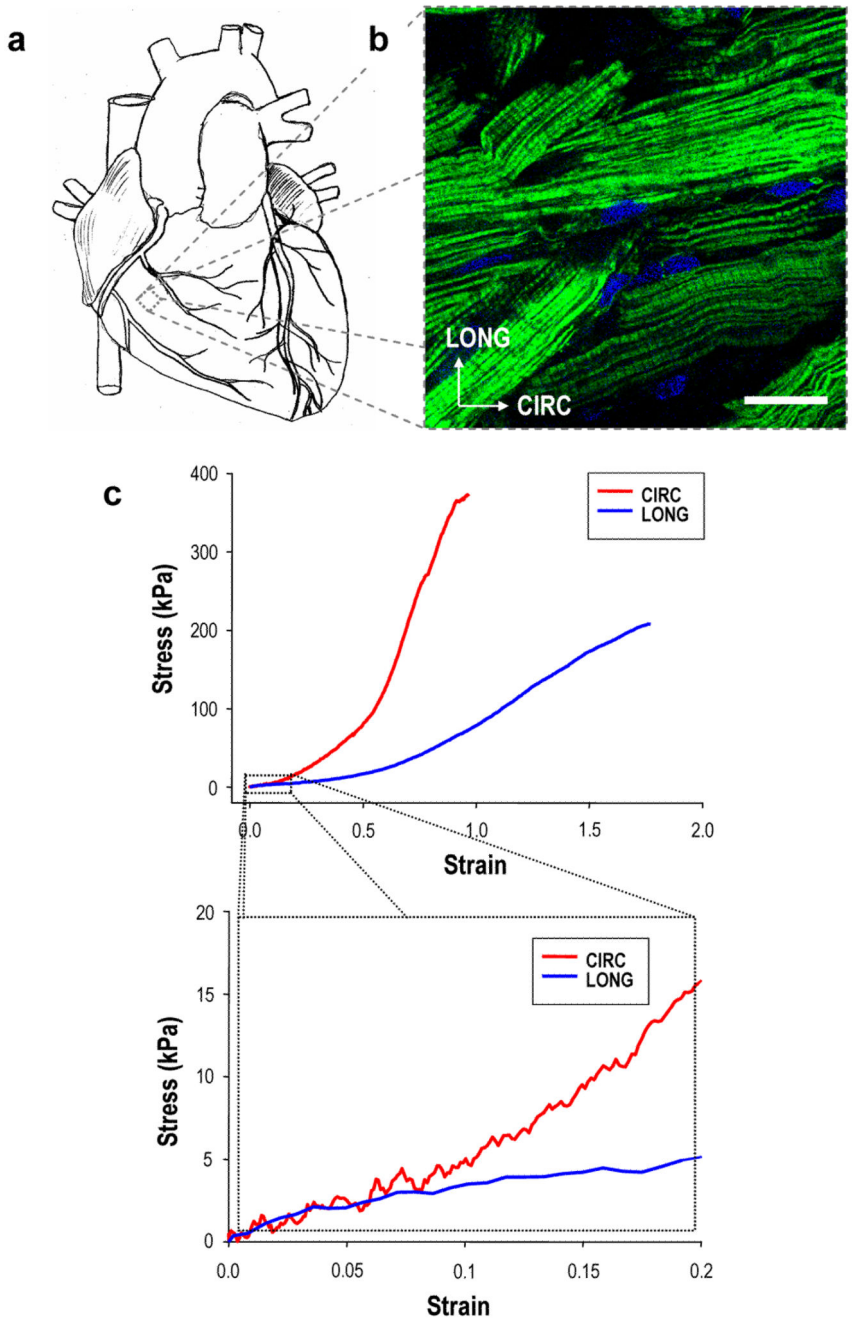

FIGURE 1. Structural and mechanical aspects of cardiac anisotropy

Ventricular myocardium has long been recognized as an anisotropic tissue, with tensile mechanical properties dictated by cardiac muscle fiber orientation. **a**, Schematic illustrating the gross macroscopic appearance of a four chamber mammalian heart. **b**, Full-thickness specimen of adult rat right ventricular (RV) myocardium showing preferentially oriented cardiac muscle fibers, fluorescently labeled for filamentous (F-) actin and cell nuclei and imaged from the epicardial surface by confocal microscopy. Scale bar = 50 μm; anatomically defined circumferential (CIRC) and longitudinal (LONG) axes are indicated. **c**,

Representative uniaxial tensile stress-strain plots for CIRC and LONG specimens of full-thickness RV myocardium demonstrated anisotropic mechanical properties consistent with observed cell orientations (upper panel = full range to demonstrate failure properties; lower panel = physiologic regime19–21). Collectively, these structural, mechanical, and associated electrical properties comprise the interrelated aspects of cardiac anisotropy.

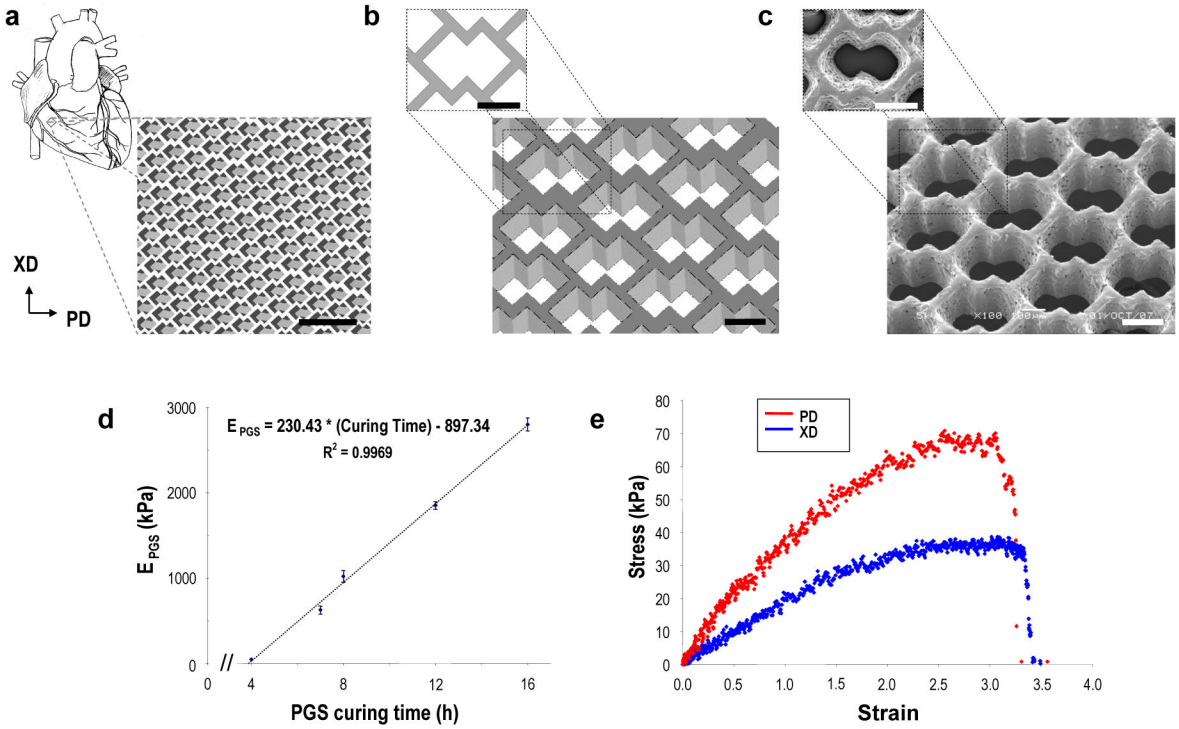

FIGURE 2. Accordion-like honeycomb scaffolds yield anisotropic mechanical properties similar to native myocardium

a, **b**, Schematics illustrating the accordion-like honeycomb design constructed by two overlapping 200 × 200 μm squares rotated 45° (i.e., diamonds). Preferred (PD) and orthogonal cross-preferred (XD) material directions, respectively corresponding to CIRC and LONG axes of the heart (Fig. 1), are indicated. Scale bars = 1 mm (**a**) and 200 μm (**b**). **c**, Scanning electron micrographs demonstrating the fidelity of excimer laser microablation in rendering an accordion-like honeycomb designs in poly(glycerol-sebacate) (PGS). Scale bars = 200 μm. **d**, PGS curing time was systematically varied, yielding a linear dependence of PGS effective stiffness (E_{PGS}) on curing time within the tested range. **e**, Representative uniaxial stress strain plots for accordion-like honeycomb scaffolds with cultured neonatal rat heart cells (scaffolds were fabricated from PGS membranes cured for 7.5h at 160°C; neonatal rat heart cells were cultured for 1 week).

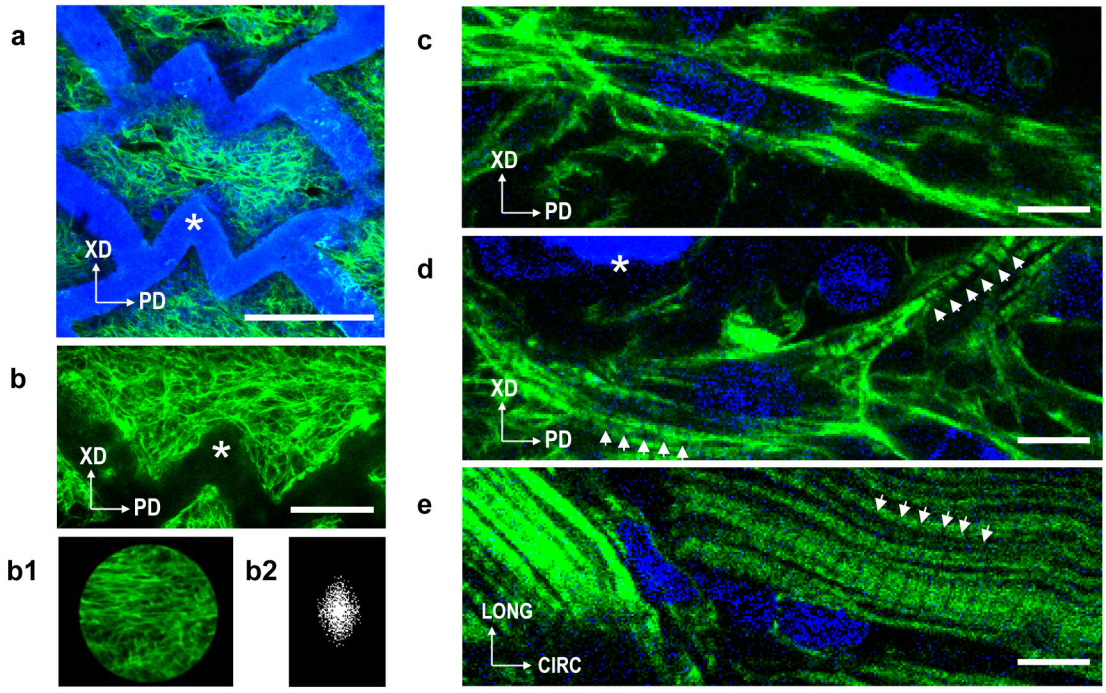

FIGURE 3. Accordion-like honeycomb scaffolds guide heart cell alignment

a-d, Neonatal rat heart cells were cultured for 1 week on accordion-like honeycomb scaffolds, fluorescently labeled for filamentous (F-) actin (green), counterstained for nuclear DNA (blue), and imaged by confocal microscopy to assess cell morphology and alignment by Fast Fourier Transform (FFT) analysis40,51. Note that F-actin labeling principally identified stress fibers in the cardiac fibroblast fraction of the cultured neonatal heart cells. **a**,**b**, Low magnification images of a representative graft demonstrated pores completely filled by neonatal rat heart cells grossly aligned in parallel to the PD direction. Insets **b1–b2**, cell alignment was quantified by cropping confocal micrographs using a circular mask, and determining F-actin orientation distribution in the associated FFT images (see Supplemental Information, Fig. S6–S11). **c,d,** Higher magnification images of neonatal rat heart cells cultured on scaffolds (**c,d**) demonstrating presence of some elongated neonatal rat heart cells and cross-striations (**d,** white arrows) similar but significantly less developed than those present in **e,** control specimens of adult rat RV myocardium (a magnification of Fig. 1b). Scale bars 200 μm (**a**); 100 μm (b); 10 μm (**c,d,e**). Scaffold is indicated by the white asterisks.

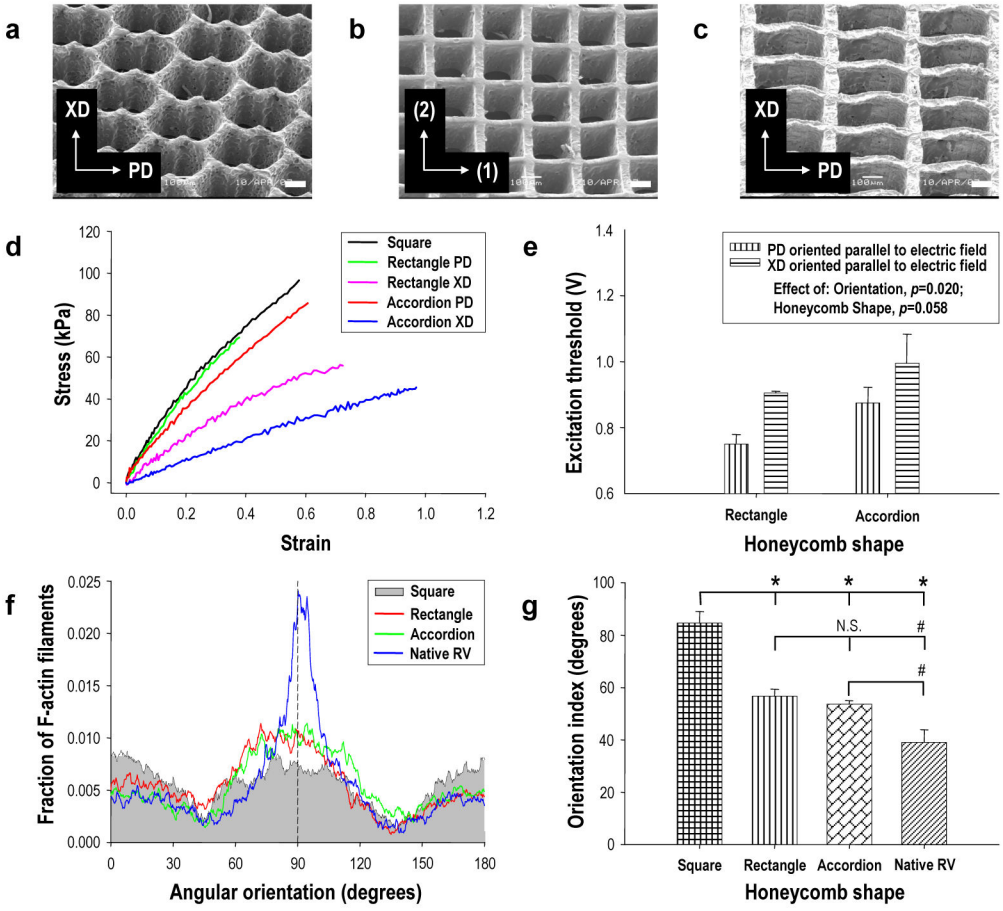

FIGURE 4. Anisotropic honeycomb scaffolds promote heart cell alignment and directionally dependent electrophysiologic properties

a–c, Scanning electron micrographs of (**a**) accordion-like, (**b**) square, and (**c**) rectangular honeycomb scaffolds. Scale bars 100 μm: Axes show (a,c) preferred (PD) and cross-preferred (XD) material directions or (b) are arbitrarily labeled (1) and (2). **d**, Comparison of the uniaxial stress-strain behaviors of scaffolds with different honeycomb microstructures, demonstrating anisotropic mechanical response of the accordion-like and rectangular honeycomb scaffolds versus the isotropic mechanical response of square honeycomb scaffolds. **e**, Electrical field stimulation demonstrated directionally dependent excitation thresholds (ET) for grafts based on anisotropic scaffolds. ET was significantly lower ($p=0.02$) when the scaffold PD was oriented parallel to the electric field, with no consistent differences observed in isotropic square honeycombs (data not shown). Data represent mean ± SEM for n=4 specimens. **f,g**, FFT-analysis of confocal images demonstrated preferential cell alignment in grafts based on anisotropic scaffolds. **f**, Plots of the mean fraction of F-actin filaments versus angular orientation. The PD orientation was arbitrarily designated as 90° (black dashed line), and an orientation index (OI) was defined as the angular increment about the distribution mean encompassing 50% of the F-actin filament population. **g**, OI data demonstrated that anisotropic honeycomb scaffolds induced a significantly higher degree of heart cell alignment than isotropic honeycombs, albeit lower cell alignment than adult rat

RV. Data are mean ± SEM for n=6 pores from a representative specimen from each group. * $p < 0.0001$. # $p < 0.05$. N.S. indicates “not significant.”

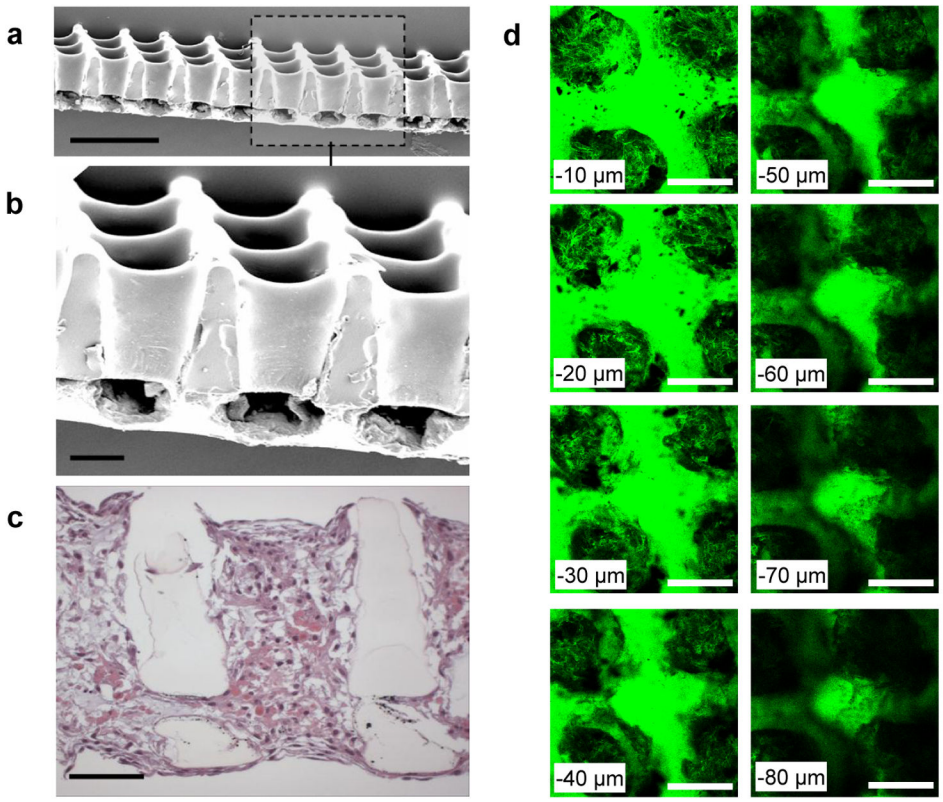

FIGURE 5. Prototype bilaminar honeycomb scaffolds with 3-D interconnected pore networks are compatible with heart cell cultivation

Prototype bilaminar honeycomb scaffolds with 3-D pore networks were fabricated from PGS via a combination of excimer laser microablation and lamination. **a**,**b**, Scanning electron micrographs of bilaminar scaffolds with fully interconnected 200 μm × 200 μm top-to-bottom and ~200 μm × 100 μm lateral pores. **c,** Cross-section of a bilaminar honeycomb scaffold with cultured neonatal rat heart cells stained by hematoxylin and eosin. Histology demonstrated the presence of interconnected neonatal rat heart cells throughout the scaffold, spanning and penetrating its pores, and elongated near the scaffold surfaces. **d**, Serial confocal sections of an F-actin labeled bilaminar scaffold with cultured neonatal rat heart cells provided an additional perspective of the lateral pore interconnectivity. Serial confocal sections begin 10 μm in from the bottom surface (top-left panel) and end 80 μm in from the bottom surface (bottom-right panel). Scale bars (**a**) 500 μm; (**b–d**) 100 μm.

Table 1

Summary of the effective stiffnesses (E_{PD}, E_{XD}), anisotropy ratio (E_{PD}/E_{XD}), and strains-to-failure (εf_{PD}, εf_{XD}) measured in uniaxial tension for accordion-like honeycomb scaffolds (cured 7.5h/160°C) under various conditions: 24 h wetting in water, 3 week wetting in water, 1 week fatigue by cyclic uniaxial stretch (1 Hz, 0.1 strain) in buffered saline, and 1 week culture with unseparated neonatal rat heart cells. Corresponding data measured for native adult rat right ventricle (RV) is shown for comparison. Scaffold PD and XD directions respectively correspond to the CIRC and LONG axes of the myocardium.

	Accordion-like honeycomb scaffolds, PGS 7.5h/160°C				
Parameter	24 h wet (n=3)	3 wks wet (n=3)	1 wk fatigue (n= 3)	1 wk heart cells (n= 5)	Adult rat RV myocardium (n=4)
E_{PD} (kPa)	83 ± 2 *a,b,c,d*	85 ± 7 *a,b,c,d*	46 ± 4 *a*	32 ± 2 *d*	54 ± 8 *a*
E_{XD} (kPa)	31 ± 1	33 ± 2	19 ± 0.8	19 ± 4	20 ± 4
E_{PD}/E_{XD}	2.7 ± 0.1	2.6 ± 0.1	2.4 ± 0.2	1.9 ± 0.3	2.8 ± 0.5
εf_{PD}	1.6 ± 0.2	1.9 ± 0.3 *d*	2.1 ± 0.3 *d*	2.4 ± 0.2 *d*	0.9 ± 0.1
εf_{XD}	1.6 ± 0.02 *c*	2.0 ± 0.1	1.3 ± 0.2	2.7 ± 0.2 *d*	1.3 ± 0.2

Data represent mean ± SEM.

a significantly different from corresponding sample tested in the orthogonal direction.

b significantly different from corresponding fatigued sample.

c significantly different from corresponding sample with cultured cells.

d significantly different from adult rat RV myocardium.